NATIONAL ADVISORY COMMITTEE FOR AERONAUTICS

TECHNICAL NOTE 2986

EFFECT OF BLADE-THICKNESS TAPER ON AXIAL-VELOCITY DISTRIBUTION AT THE LEADING EDGE OF AN ENTRANCE ROTOR-BLADE ROW WITH AXIAL INLET, AND THE INFLUENCE OF THIS DISTRIBUTION ON ALINEMENT OF THE ROTOR BLADE FOR ZERO ANGLE OF ATTACK

By John D. Stanitz

Lewis Flight Propulsion Laboratory
Cleveland, Ohio

Washington
August 1953

NATIONAL ADVISORY COMMITTEE FOR AERONAUTICS

TECHNICAL NOTE 2986

EFFECT OF BLADE-THICKNESS TAPER ON AXIAL-VELOCITY DISTRIBUTION AT THE LEADING EDGE OF AN ENTRANCE ROTOR-BLADE ROW WITH AXIAL INLET, AND THE INFLUENCE OF THIS DISTRIBUTION ON ALINEMENT OF THE ROTOR BLADE FOR ZERO ANGLE OF ATTACK

By John D. Stanitz

SUMMARY

A method is developed for estimating the effect of blade-thickness taper on the inlet axial-velocity distribution of an entrance rotor-blade row with axial inlet, and the influence of this velocity distribution on the alinement of the rotor blade for zero effective angle of attack (that is, zero blade loading at the nose). This alinement of the blade requires a deviation between the angle of the blade camber line direction at the inlet and the upstream relative flow direction. The method is developed for compressible and incompressible nonviscous fluids, and results are presented for incompressible flow into a plane, two-dimensional cascade and for compressible flow into an entrance rotor-blade row with tapered blades. It is concluded that, for the entrance rotor-blade row investigated, blade taper has a large effect on the inlet deviation angle; whereas compressibility has a small effect, except perhaps at the hub, and the upstream relative flow direction also has a small effect.

INTRODUCTION

If the blade-element profile is to be set at the desired angle of attack at each radius in any blade row of a turbomachine, it is first necessary to know the blade-element alinement for zero "effective" angle of attack, that is, for zero loading at the inlet. In many cases this alinement is considerably different from the upstream relative flow direction, and if it is not known, improper angles of attack may result. Thus, rapid blade loading, accompanied by high peak velocities near the nose of the blade-element profile, may occur. The subsequent deceleration from these high velocities on the blade surface can result in local boundary-layer separation and accompanying mixing losses. For a blade

row with an essentially blunt leading edge, the gas passes from the "approach" station, which is immediately upstream of the blade leading edge, to the "inlet" station, which is immediately downstream of the blade leading edge and has finite "effective" blade thickness. Alinement of the blade-element profile for zero angle of attack, that is, for essentially zero loading at the inlet station, will depend on the inlet axial velocity (at the inlet station) and must be such that the whirl (product of absolute tangential velocity and radius) is unchanged from its upstream value along the same streamline. For "entrance" rotor-blade rows, which are not preceded by guide vanes and which are the subject of this report, the upstream whirl is zero. For this type of rotor-blade row, which occurs in centrifugal- and axial-flow compressors that do not have inlet guide vanes, the zero angle of attack condition is achieved when the blade profile at each radius is alined to preserve zero whirl at the inlet station immediately downstream of the leading edge.

In the design of entrance rotor-blade rows with axial inlets it is common practice, although usually incorrect, to assume a uniform approach axial-velocity distribution. Actually there are a number of factors that can result in nonuniform distributions. Among these factors are: (1) boundary layer on the hub and casing, (2) meridional curvature of the hub and casing upstream and/or downstream of the blade leading edge, (3) blade curvature, (4) radial variations in angle of attack, and (5) blade taper (radial variation in blade thickness).

The influence of boundary layer on the approach axial-velocity distribution is obvious; likewise, meridional curvatures of the hub and casing should be expected to cause nonuniform distributions in which the highest velocities occur at the walls with larger convex curvature. The effect of hub and casing curvatures downstream of the blade leading edge, such as occur in centrifugal and mixed-flow compressors, has been noted in reference 1. Blade curvature and radial variations in angle of attack can result in radial displacements of the meridional streamlines, which induce nonuniform approach axial-velocity distributions. Likewise, blade taper requires radial displacements of the flow and therefore induces variations in the approach axial-velocity distribution.

It will be assumed that the approach axial-velocity variations, and therefore the inlet axial-velocity variations, induced by these various factors can be treated separately, and that the resulting distribution can be determined with reasonable accuracy by a simple superposition of the several variations. It is, then, the purpose of this report to investigate, analytically, the variation in inlet axial-velocity distribution due to blade taper alone, and to indicate the influence of this distribution on the alinement of the rotor blade-element profile for zero angle of attack at each radius. The investigation includes both compressible and incompressible fluids; for compressible fluids the

condition of sonic relative velocity at the inlet station is also considered. The object of this investigation, made at the NACA Lewis laboratory, is to obtain approximate values of the phenomena involved and improved knowledge of the physical mechanisms.

METHOD OF ANALYSIS

A method is developed for estimating the variation in inlet axial-velocity distribution induced by the blade taper in an entrance rotor-blade row. In addition, a method is developed for estimating corrections to the rotor-blade inlet angles so that the blade is alined with the flow, that is, so that the blade loading is approximately zero at the inlet.

Preliminary Considerations

Statement of problem. - If all factors except blade taper affecting the inlet axial-velocity distribution in an entrance rotor-blade row are eliminated, the problem of the inlet axial-velocity distribution reduces to axial flow through an annulus of concentric circular cylinders in which is located a cascade of straight blades with specified taper lying, in effect (see appendix B), in the meridional (axial-radial) plane and extending downstream to infinity. Such an annulus is shown in figure 1 together with a meridional streamline that is displaced radially outward by the blade taper. (The symbols used in fig. 1 and elsewhere in this report are defined in appendix A.) Far upstream and downstream of the blade leading edge the streamlines are parallel to the axis and the axial velocity is uniform from hub to casing. In the vicinity of the leading edge, however, the radial displacement of the streamlines induces a variation in axial-velocity distribution from hub to casing at both the approach and the inlet stations. This variation in velocity distribution depends on, and will be estimated for, specified values of the uniform upstream velocity, blade taper, and hub-tip ratio. The variation in inlet axial-velocity distribution requires an adjustment from hub to tip in the rotor-blade inlet angle β_i (inlet station, fig. 1) in order to achieve zero blade loading at the inlet.

Assumptions. - As already stated, it is assumed that the effects of blade taper on the inlet axial-velocity distribution can be treated (with reasonable accuracy) separately from the effects of other factors, and that the resultant effect of all factors can be determined by simple superposition. (However, only the effect of blade taper is considered herein.) In addition, the flow is assumed to be axially symmetric. Also, the leading edge of the blade is assumed essentially blunt (fig. 1), although shaped to avoid entrance losses. Both compressible (subsonic) and incompressible nonviscous fluids are considered. Further assumptions are introduced as needed.

Outline of method. - The variation in inlet axial-velocity distribution that results from blade taper in an entrance rotor-blade row is obtained from a stream function distribution at the inlet station that is related, by assumption, to the known upstream and downstream distributions. (The validity of this assumption is checked in appendix B.) After the inlet axial-velocity distribution from hub to casing is known, the inlet deviation angle ϵ_i (inlet station, fig. 1) of the rotor-blade inlet angle β_i from the upstream relative flow direction β_u is determined in such a way that the absolute tangential velocity is unchanged (zero), that is, so that the blade is not loaded at the inlet. It is supposed that knowledge of this deviation angle is needed, as a reference, in order to set the blade-element profile at the desired angle of attack.

Coordinates and velocity components. - A point between the hub and casing in the meridional plane is designated by its r,z coordinates, where r is measured from the axis of the annulus and z is measured from the leading edge of the blade, positive in the direction of flow (fig. 1). These coordinates are dimensionless, being expressed as ratios of the casing radius (so that r is 1.0 at the blade tip, for example). The hub radius is designated by r_h.

The velocity components in the r and z directions are v and u, respectively. These velocity components are dimensionless, being expressed for incompressible flow as ratios of the upstream velocity (so that for incompressible flow u_u is equal to 1.0, for example), and being expressed for compressible flow as ratios of the upstream stagnation speed of sound.

The angular velocity ω of the rotor is dimensionless, being expressed in such a way that the dimensionless wheel speed ωr is a ratio of the upstream velocity for incompressible flow and a ratio of the upstream stagnation speed of sound for compressible flow.

As a result of the wheel speed, the flow relative to the rotor has the direction β measured from the axial direction on a developed cylindrical surface (fig. 1). The difference between the upstream relative flow direction β_u and the relative flow direction β is defined as the deviation angle ϵ (fig. 1).

$$\epsilon = \beta_u - \beta \tag{1}$$

Blade taper. - The blade taper is determined by the variation in the passage width ratio δ, which is defined at each radius as the ratio of the circumferential passage width between adjacent blades to the blade spacing (fig. 1). Thus, if σ is the angular spacing of the

blades about the z-axis, $\delta r\sigma$ is the passage width, and the circumferential blade thickness t is given by (fig. 1)

$$t = (1-\delta)\, r\sigma \tag{2}$$

Thus, if the blade taper is defined as $-(dt/dr)$, equation (2) results in

$$-\frac{dt}{dr} = \left[\frac{d(\delta r)}{dr} - 1\right]\sigma \tag{3}$$

In this report the passage width ratio δ will be specified as a function of r by the power series

$$\delta = a + br + cr^2 + \ldots \tag{4}$$

Inlet Axial-Velocity Distribution

Stream function Ψ. - As a result of continuity considerations a stream function Ψ is defined (appendix B) such that

$$\frac{\partial \Psi}{\partial r} = \frac{\delta r \rho u}{\Delta \psi} \tag{5}$$

where for isentropic flow the density ρ is given by

$$\rho = \left(1 - \frac{\gamma-1}{2}\, u^2\right)^{\frac{1}{\gamma-1}} \tag{6}$$

and where, in terms of upstream flow conditions,

$$\Delta\psi = \rho_u u_u \left(\frac{1-r_h^2}{2}\right) \tag{7a}$$

or, in terms of downstream flow conditions,

$$\Delta\psi = \rho_d u_d \, \frac{a}{2}\left[(1-r_h^2) + \frac{b}{3}(1-r_h^3) + \frac{c}{4}(1-r_h^4) + \ldots\right] \tag{7b}$$

The stream function Ψ has been defined (by the introduction of $\Delta\psi$) so that it varies from 0 to 1.0 between the hub and the casing, respectively. The density ρ is dimensionless, being expressed as a ratio of the upstream stagnation density. For incompressible flow ρ is 1.0.

Upstream distribution of Ψ. - Far upstream of the blade inlet, both ρ and u are constant and δ is 1.0; so that equation (5) can be integrated to give, when combined with equation (7a),

$$\Psi_u = 1 - \frac{1-r^2}{1-r_h^2} \tag{8}$$

Equation (8) gives the upstream distribution of Ψ as a function of r.

Downstream distribution of Ψ. - Far downstream of the blade inlet, both ρ and u are constant (because all factors other than blade taper have been neglected) and δ is given by equation (4); so that equation (5) can be integrated to give, when combined with equation (7b),

$$\Psi_d = 1 - \frac{\frac{a}{2}(1-r^2) + \frac{b}{3}(1-r^3) + \frac{c}{4}(1-r^4) + \ldots}{\frac{a}{2}(1-r_h^2) + \frac{b}{3}(1-r_h^3) + \frac{c}{4}(1-r_h^4) + \ldots} \tag{9}$$

Equation (9) gives the downstream distribution of Ψ as a function of r.

Inlet distribution of Ψ. - At the blade inlet, both ρ and u are unknown and variable and δ changes suddenly from an upstream value of 1.0 to its prescribed downstream values. Under these unknown conditions equation (5) cannot be integrated; instead it is assumed that the inlet value of Ψ at each radius is equal to the average of its upstream and downstream values at the same radius.

$$\Psi_i = \frac{1}{2}(\Psi_u + \Psi_d) \tag{10}$$

This basic assumption is shown to be valid by a series of relaxation solutions in appendix B. Because the density is constant at both the upstream and downstream stations, the distributions of Ψ_u and Ψ_d are independent of compressibility effects (see eqs. (8) and (9)). Equation (10) therefore assumes that Ψ_i is also independent of compressibility effects. Inasmuch as the density is not constant at the inlet station, this assumption is also investigated in appendix B.

Inlet axial-velocity distribution. - The inlet axial-velocity distribution is obtained from the radial derivative of the distribution of Ψ_i given by equation (10). Thus, from this derivative and equations (5), (7a), (8), and (9),

$$\rho_i u_i = \frac{\rho_u u_u}{4}\left[\frac{2}{\delta} + \frac{1-r_h^2}{\frac{a}{2}(1-r_h^2) + \frac{b}{3}(1-r_h^3) + \frac{c}{4}(1-r_h^4) + \cdots}\right] \quad (11)$$

The distribution of u_i from hub to casing is given by equation (11) in which ρ_i is related to u_i by equation (6) and δ is a specified function of r given by equation (4).

Rotor-Blade Alinement

A method is developed for computing the radial variation in inlet deviation angle ϵ_i required to avoid loading of entrance rotor blades at the inlet. Although the method, as developed, takes into account the effects of blade taper only, it can be extended, by methods to be discussed later, to include the effects of other factors.

Inlet deviation angle ϵ_i. - For an entrance rotor blade the relative upstream flow direction β_u is given by (fig. 1)

$$\tan \beta_u = \frac{\omega r}{u_u} \quad (12)$$

(In order to avoid negative values of β, ωr is considered positive as shown in fig. 1.) Equation (12) can also be expressed as

$$\tan \beta_u = r(\tan \beta_u)_{1.0} \quad (12a)$$

where the subscript 1.0 refers to the casing at which r is 1.0. At the blade inlet, immediately downstream of the leading edge,

$$\tan \beta_i = \frac{\omega r}{u_i}$$

which, from equation (12), becomes

$$\tan \beta_i = \frac{u_u}{u_i} \tan \beta_u \quad (13)$$

Also, from equation (1),

$$\tan \epsilon_i = \frac{\tan \beta_u - \tan \beta_i}{1 + \tan \beta_u \tan \beta_i}$$

which, from equation (13), becomes

$$\tan \epsilon_i = \frac{\left(1 - \frac{u_u}{u_i}\right) \tan \beta_u}{1 + \frac{u_u}{u_i} \tan^2 \beta_u} \tag{14}$$

The distribution of inlet deviation angle ϵ_i from hub to casing is given by equation (14), in which u_i is given by equation (11) and β_u is given by equation (12a).

Special case. - If the flow is plane and incompressible, r_h and ρ are 1.0, and equation (11) reduces to

$$u_i = \frac{u_u}{\delta}$$

so that equation (14) reduces to

$$\tan \epsilon_i = \frac{(1 - \delta) \tan \beta_u}{1 + \delta \tan^2 \beta_u} \tag{15}$$

Equation (15) has been developed by Weinig (ref. 2, p. 120).

Condition for sonic inlet relative velocity. - It can be shown that, if the blades are alined for zero loading at the nose, the resultant inlet relative velocity is sonic when

$$(\omega r)^2 + \frac{\gamma+1}{2} u_i^2 = 1$$

which, from equation (12), becomes

$$u_i^2 = \frac{2}{\gamma+1} (1 - u_u^2 \tan^2 \beta_u) \tag{16}$$

From equations (6), (11), and (16),

$$4\sqrt{\frac{2}{\gamma+1}\left(\frac{1}{u_u^2}-\tan^2\beta_u\right)}\left[\frac{1-\frac{\gamma-1}{\gamma+1}\left(1-u_u^2\tan^2\beta_u\right)}{1-\frac{\gamma-1}{2}u_u^2}\right]^{\frac{1}{\gamma-1}}=\frac{2}{\delta}+\frac{1-r_h^2}{\frac{a}{2}\left(1-r_h^2\right)+\frac{b}{3}\left(1-r_h^3\right)+\frac{c}{4}\left(1-r_h^4\right)+\ldots} \tag{17}$$

Equation (17) is the condition for which the resultant relative inlet velocity is sonic. This condition is of interest, as a limit, if the designer wishes to avoid supersonic inlet relative velocities.

Numerical Procedure

Specified conditions. - In order to investigate the effect of blade taper on the inlet axial-velocity distribution of an entrance rotor-blade row and the influence of this distribution on the inlet deviation angle ϵ_i, the following conditions must be specified:

$$\left.\begin{array}{l}(\tan\beta_u)_{1.0}\\ u_u\\ r_h\\ \delta=\delta(r)\end{array}\right\} \tag{18}$$

For compressible flow u_u is expressed as a ratio of the upstream stagnation speed of sound; for incompressible flow u_u is 1.0. The specified distribution of δ as a function of r is given by the coefficients $a, b, c, \ldots$ in equation (4). The specified distribution of δ is related to the blade taper $-(dt/dr)$ by equation (3).

Calculations. - The following procedure is used in the calculations:

(1) If the fluid is compressible, and if the designer wishes to avoid supersonic inlet relative velocities, the conditions (u_u and β_u)

for which the inlet relative velocity is sonic should be determined from equation (17).

(2) If from step (1) the assigned value of u_u does not result in sonic relative velocity, compute u_i from equation (11) in which ρ is related to u by equation (6). If the fluid is incompressible, ρ is 1.0.

(3) Compute ϵ_i from equation (14).

If other factors besides blade taper affect u_i and ϵ_i, it is first necessary to compute the approach axial-velocity distribution u_a (at the approach station, fig. 1) resulting from each of these factors considered separately. For example, the approach axial-velocity distribution u_a resulting from blade taper alone is given by the continuity equation

$$\rho_a u_a = \delta \rho_i u_i \tag{19}$$

where $\rho_i u_i$ is given by equation (11) and ρ_a is related to u_a by equation (6). The variations in u_a from u_u that result from each of the factors separately are then added to obtain the resultant distribution of u_a. The final distribution of u_i is then obtained from equation (19), using the resultant distribution of u_a, and the distribution of inlet deviation angle ϵ_i is then determined by equation (14).

RESULTS AND DISCUSSION

Results are presented for incompressible flow into a plane, two-dimensional cascade and for compressible flow into an entrance rotor-blade row with tapered blades.

Plane cascade with incompressible flow. - For incompressible flow into a plane, two-dimensional cascade, equation (15), developed by Weinig, relates the inlet deviation angle ϵ_i to the upstream flow direction β_u and the passage width ratio δ. The relation is plotted in figure 2. As expected, ϵ_i increases with decreasing values of δ. It is interesting to note that for values of δ commonly occurring in practice, say 0.7 or greater, the values of ϵ_i are 10° or less. For values of δ as low as 0.5, such as might occur near a blade root, the values of ϵ_i can be as high as 20°.

Entrance rotor-blade row with blade taper. - The more general case of compressible flow into an entrance rotor-blade row with the same hub-tip ratio and blade taper used in example V of appendix B is considered. First, in order to avoid specifying upstream flow conditions (u_u and $(\beta_u)_{1.0}$) that result in local sonic flow at the inlet station, the critical value of u_u (at each radius) for which the relative inlet velocity is sonic, determined by equation (17), is plotted in figure 3 as a function of r for three values of $(\beta_u)_{1.0}$. The variation in this critical value of u_u with r in figure 3 is not large for this thickness distribution, because the blade speed increases the inlet relative velocity toward the casing and the blade taper increases the velocity toward the hub. (This taper effect must be large because, as will be shown, ϵ_i increases toward the hub and this increase tends to reduce the inlet relative velocity there.) For $(\beta_u)_{1.0}$ equal to 60° the variation in u_u with r lies between 0.45 and 0.50, indicating that sonic relative velocity occurs almost simultaneously from hub to casing. For $(\beta_u)_{1.0}$ equal to 50°, sonic inlet relative velocity first appears at the hub (as indicated by the minimum value of u_u at this radius); whereas for $(\beta_u)_{1.0}$ equal to 70°, sonic velocity first appears at the casing.

The variation in inlet deviation angle ϵ_i with radius for various values of u_u and $(\beta_u)_{1.0}$ was determined by equations (11) and (14) and is plotted in figure 4. In figure 4(a) the effect of u_u on ϵ_i is shown for $(\beta_u)_{1.0}$ equal to 60°. A maximum value of 0.4 for u_u was chosen in order to avoid the sonic inlet relative velocity predicted by figure 3. The higher values of ϵ_i toward the hub indicate a large effect of blade taper on ϵ_i. The spread in the curves for various values of u_u indicates that, for the example investigated, the effect of compressibility on ϵ_i is not important, except perhaps near the hub (where, however, the relaxation solutions in appendix B show that the estimated values of u_i (and therefore ϵ_i) are too high, especially for high subsonic values of u_i).

In figure 4(b) the effect of $(\beta_u)_{1.0}$ on ϵ_i is shown for u_u equal to 0 (corresponding to incompressible flow). Again the curves indicate a large effect of blade taper on ϵ_i. The spread in the curves for various values of $(\beta_u)_{1.0}$ indicates that for the example investigated the effect of $(\beta_u)_{1.0}$ on ϵ_i is not important. This result

agrees with that for plane cascades with incompressible flow where (fig. 2), for the range of δ considered in figure 4(b), only small variations in ϵ_i occur for large variations in β_u. However, as the value of δ decreases it is observed in figure 2 that the influence of β on ϵ_i becomes more pronounced.

Further considerations. - In the practical application of the methods developed in this report for estimating the radial variation in ϵ_i, certain difficulties may arise with regard to the selection of δ as a function of r. These difficulties arise if the blade nose is faired (fig. 5), instead of being blunt (fig. 1), so that δ is a function of z as well as of r. In this case it is necessary to assume some "effective" variation in δ with r, which might, for example, be the variation 2 or 3 percent of the blade height downstream of the blade leading edge. Another difficulty, discussed in appendix B, is the breakdown for high values of u_i in the basic assumption that u_i can be computed from the distribution of Ψ_i given by equation (10). In both these cases, however, the estimated values of u_a, u_i, and ϵ_i can serve as a guide to the designer (if properly interpreted).

In this analysis it has been assumed that the blade-element profiles have blunt noses (or, in the event that the noses are not blunt, that some "effective" blade thickness can be assumed). It is therefore of interest to examine the inlet profiles that Weinig (ref. 2) has developed for the type of two-dimensional cascade blades considered in figure 2. These profiles have been developed to give a continually accelerating flow from the stagnation point at the nose to the maximum velocity in the downstream channel between blades. Such a velocity distribution eliminates the possibility of local boundary-layer separation near the nose. From equations on page 122 of reference 2, the profile coordinates, x along the blade chord and y normal to the chord, are given by

$$x = \frac{\delta \cos \beta_i}{\pi} \left\{ \ln \sec \left[\frac{\pi y}{(1-\delta) \cos \beta_i} - \beta_u \right] + \left[\frac{\pi y}{(1-\delta) \cos \beta_i} - \beta_u \right] \tan \beta_u \right\} \tag{20}$$

where, for the type of cascade being considered,

$$\tan \beta_i = \delta \tan \beta_u \tag{21}$$

and where the x and y coordinates are expressed as ratios of the circumferential blade spacing. Examples of the blade profiles are given in figure 5 for three values of δ and for β_u equal to 45°. The

radius of curvature R at the blade nose, expressed as a ratio of the circumferential blade spacing, is given by (ref. 2, p. 121)

$$R = \frac{\delta(1-\delta)^2 \cos \beta_i}{\pi(\delta^2 + \tan^2 \beta_i)} \tag{22}$$

This radius might be of some help in approximating the desired blade-element profile, and it is therefore plotted in figure 6 as a function of δ for various values of β_u.

SUMMARY OF RESULTS AND CONCLUSIONS

A method is developed for estimating the effect of blade taper on the inlet axial-velocity distribution of an entrance rotor-blade row with axial inlet and the influence of this velocity distribution on the alinement of the rotor blade for zero loading at the nose. This alinement of the blade results in an inlet deviation angle ϵ_i of the blade-camber-line direction at the inlet from the upstream relative flow direction. The method applies to both compressible and incompressible nonviscous flows, and an expression is developed for predicting local sonic relative velocity at the inlet. The method is applied to plane, two-dimensional cascades with incompressible flow and to the more general problem of compressible flow into an entrance rotor-blade row with blade taper. It is concluded that for the entrance rotor-blade row investigated:

1. Blade taper has a large effect on ϵ_i.

2. The effect of compressibility on ϵ_i is small, except near the hub.

3. The effect of upstream relative flow direction on ϵ_i is small.

4. The upstream velocity for which the relative inlet velocity is sonic at a given radius does not vary greatly from hub to casing. (In one example sonic relative velocity occurred almost simultaneously from hub to casing.)

Lewis Flight Propulsion Laboratory
National Advisory Committee for Aeronautics
Cleveland, Ohio, May 19, 1953

APPENDIX A

SYMBOLS

The following symbols are used in this report: (All symbols are dimensionless; velocities are expressed as ratios of the upstream absolute stagnation speed of sound for compressible flow, and as ratios of the upstream axial velocity for incompressible flow; distances are expressed as ratios of the casing radius, unless otherwise specified.)

$a,b,c, \ldots$	coefficients, prescribed to define δ by eq. (4)
R	radius at nose of two-dimensional blade profile, expressed as ratio of blade spacing in two-dimensional cascade, eq. (22)
r	radius, measured from axis of annulus, fig. 1
t	circumferential blade thickness, eq. (2)
u,v	axial and radial velocities, respectively
x,y	coordinates of two-dimensional blade profile, measured along blade chord and normal to it, respectively, and expressed as a ratio of blade spacing in two-dimensional cascade, eq. (20)
z	axial distance, measured from leading edge of blade, positive in direction of flow, fig. 1
β	relative flow angle, fig. 1
γ	ratio of specific heats
δ	passage width ratio, ratio of circumferential passage width to circumferential blade spacing at same radius
ϵ	deviation angle, eq. (1)
ρ	density, expressed as ratio of upstream stagnation density, eq. (6)
σ	angular spacing of blades around z-axis, fig. 1
Ψ	stream function, eq. (B2)
$\Delta\Psi$	constant, defined by eq. (B3)

ω	angular velocity of rotor, expressed in such a way that the dimensionless wheel speed ωr is a ratio of upstream velocity for incompressible flow, and a ratio of upstream stagnation speed of sound for compressible flow

Subscripts:

a	approach, immediately upstream of blade leading edge (fig. 1)
d	downstream, far downstream of blade leading edge
h	hub
i	inlet, immediately downstream of blade leading edge (fig. 1)
u	upstream, far upstream of blade leading edge
1.0	casing, where r is 1.0

APPENDIX B

RELAXATION SOLUTIONS FOR DISTRIBUTION OF Ψ

The validity of the basic assumption that, for both compressible and incompressible flows,

$$\Psi_i = \frac{1}{2}(\Psi_u + \Psi_d) \tag{10}$$

is investigated by comparing the results of this assumption with the results of seven relaxation solutions for flow through annuli of the type shown in figure 1.

Method of Analysis

If it is assumed that the rotor blade profiles at the inlet, and, for purposes of this investigation, everywhere downstream of the blade leading edge, can be alined with the flow in such a manner that no work is done on the fluid, then the fluid motion in the meridional (axial-radial) plane is irrotational, so that

$$\frac{\partial u}{\partial r} - \frac{\partial v}{\partial z} = 0 \tag{B1}$$

Also, for axially symmetric flow, which assumes that the number of blades becomes infinite but that the blockage effect of the blades (determined by δ) is unchanged, the continuity equation becomes

$$\frac{\partial}{\partial r}(\delta r \rho v) + \frac{\partial}{\partial z}(\delta r \rho u) = 0$$

This continuity equation is satisfied by a stream function Ψ, which is defined by

$$\left.\begin{aligned} \frac{\partial \Psi}{\partial r} &= \frac{\delta r \rho u}{\Delta\psi} \\ \frac{\partial \Psi}{\partial z} &= -\frac{\delta r \rho v}{\Delta\psi} \end{aligned}\right\} \tag{B2}$$

where the density ρ is related to u and v by the usual isentropic equation

$$\rho = \left[1 - \frac{\gamma-1}{2}(u^2 + v^2)\right]^{\frac{1}{\gamma-1}}$$

and where the constant $\Delta\psi$ is defined by

$$\Delta\psi = \int_{r_h}^{1.0} \delta r \rho u \, dr \tag{B3}$$

so that the stream function Ψ varies from 0 at the hub to 1.0 at the casing. In terms of upstream flow conditions, where ρ and u are constant and δ is 1.0, equation (B3) can be integrated to give

$$\Delta\psi = \rho_u u_u \left(\frac{1-r_h^2}{2}\right) \tag{7a}$$

Also, in terms of downstream flow conditions, where ρ and u are constant and δ is specified by equation (4), equation (B3) can be integrated to give

$$\Delta\psi = \rho_d u_d \left[\frac{a}{2}(1-r_h^2) + \frac{b}{3}(1-r_h^3) + \frac{c}{4}(1-r_h^4) + \ldots\right] \tag{7b}$$

Equations (B1) and (B2) combine to give

$$\frac{\partial^2\Psi}{\partial r^2} + \frac{\partial^2\Psi}{\partial z^2} - \frac{\partial\Psi}{\partial r}\frac{\partial \ln(\delta r\rho)}{\partial r} - \frac{\partial\Psi}{\partial z}\frac{\partial \ln \rho}{\partial z} = 0 \tag{B4}$$

Equation (B4) determines the distribution of the stream function Ψ from hub to shroud, and the resulting velocity distribution is determined by equations (B2). It is noted that the form of equation (B4) is independent of the flow direction (or blade angle) β so that, in effect, the rotor blades can be considered to lie in the meridional plane, in which case they must also be stationary. That is, if the rotor blades are alined to do no work on the fluid, they have no effect on the absolute meridional flow other than that due to blade taper, which effect is the same for stationary blades lying in the meridional plane.

Numerical Procedure

Equation (B4) was solved by relaxation methods (ref. 3) for specified geometric and flow conditions. A square grid with 0.0625 spacing was used, and the finite-difference equations were based on a second-degree polynomial for Ψ. The residuals were reduced to give five-figure

accuracy for the value of Ψ at each grid point. The boundary values of Ψ were 0 and 1.0 along the hub and casing, respectively, and the relaxation solutions were extended upstream and downstream of the leading edge until flow conditions became uniform.

Numerical Results

Seven relaxation solutions were obtained for the conditions specified in the following table:

Example	u_u	r_h	δ	Comment*
I	0 (incompressible)	0.625	-0.25 + 1.2r	$\delta_h = 0.5$
II	0 (incompressible)	.625	0.0167 + 0.9333r	$\delta_h = 0.6$
III	0 (incompressible)	.625	0.2833 + 0.6667r	$\delta_h = 0.7$
IV	0 (incompressible)	.500	0.05 + 0.9r	$\delta_h = 0.5$
V	0 (incompressible)	.625	$-1.4556+4.7611r-2.3556r^2$	$\delta_h=0.6, \left(\frac{dt}{dr}\right)_{1.0}=0$
VI	0.44	.625	$-1.4556+4.7611r-2.3556r^2$	$\delta_h=0.6, \left(\frac{dt}{dr}\right)_{1.0}=0$
VII	0.52	.625	$-1.4556+4.7611r-2.3556r^2$	$\delta_h=0.6, \left(\frac{dt}{dr}\right)_{1.0}=0$

*The value of $(\delta)_{1.0}$ is 0.95 for all examples.

The streamline patterns for examples I through V (incompressible flow) are shown in figure 7. The deviations of the streamlines from their upstream and downstream radial positions are indicated by the dashed lines in the plots. The insert shows the blade thickness distribution for the specified variation in δ and for an angular blade spacing of 18°.

The streamline patterns for examples V through VII are shown in figure 8 together with contours of constant velocity ratio $(\sqrt{u^2+v^2})/u_u$. These solutions investigate compressibility effects for three values of

u_u (0, 0.44, and 0.52). The discontinuity in velocity distribution at the leading edge results from the sudden change in δ. This discontinuity becomes noticeably more severe as the value of u_u increases. Also, the large axial gradients of u downstream of the leading edge are an indication of large axial gradients of ϵ, which must exist if the blade is to remain unloaded. The largest value of u_u, 0.52, is the maximum value for which the relaxation solution would converge and corresponds to the condition of sonic velocity at the blade root. (Actually, eq. (17) with β_u equal to zero indicates a value of 0.4500 for sonic velocity on the hub at the blade leading edge. However, because grid points were not located on the blade leading edge, sonic velocity was not encountered in the relaxation solutions until u_u was greater than 0.52.)

Flow conditions along the blade leading edge as obtained from the relaxation solutions (I through VII) are compared in figures 9 and 10 with the estimated flow conditions based on the assumed relation given by equation (10). In figure 9, the estimated distribution of Ψ_i given by equation (10) is compared with the distribution of Ψ_i obtained by the relaxation solutions. The agreement is seen to be excellent. However, it is the accuracy of the radial derivative of Ψ_i, from which u_i is obtained, that is of interest. The upstream value of this derivative at a given radius divided by the inlet value at the same radius is equal to $\rho_u u_u / \delta \rho_i u_i$. The estimated distribution of this quantity, obtained from equation (11), is compared in figure 10 with the distribution obtained by the relaxation solutions. Again the agreement is satisfactory, except perhaps for large values of $\rho_u u_u / \delta \rho_i u_i$, which occur near the hub. For these values of $\rho_u u_u / \delta \rho_i u_i$ the estimated value of $\rho_i u_i$ is too large so that u_i is too high, especially for high subsonic values of u_i where, because $\rho_i u_i$ is almost constant, very large changes in u_i are required to achieve small changes in $\rho_i u_i$. However, except for high subsonic values of u_i near the hub, it is concluded that the basic assumption represented by equation (10) is valid for both compressible (subsonic) and incompressible flow.

REFERENCES

1. Ellis, Gaylord O., Stanitz, John D., and Sheldrake, Leonard J.: Two Axial-Symmetry Solutions for Incompressible Flow Through A Centrifugal Compressor with and without Inducer Vanes. NACA TN 2464, 1951.

2. Weinig, F.: Die Strömung um die Schaufeln von Turbomachinen. Johann Ambrosius Barth (Leipzig), 1935.

3. Southwell, R. V.: Relaxation Methods in Theoretical Physics. Clarendon Press (Oxford), 1946.

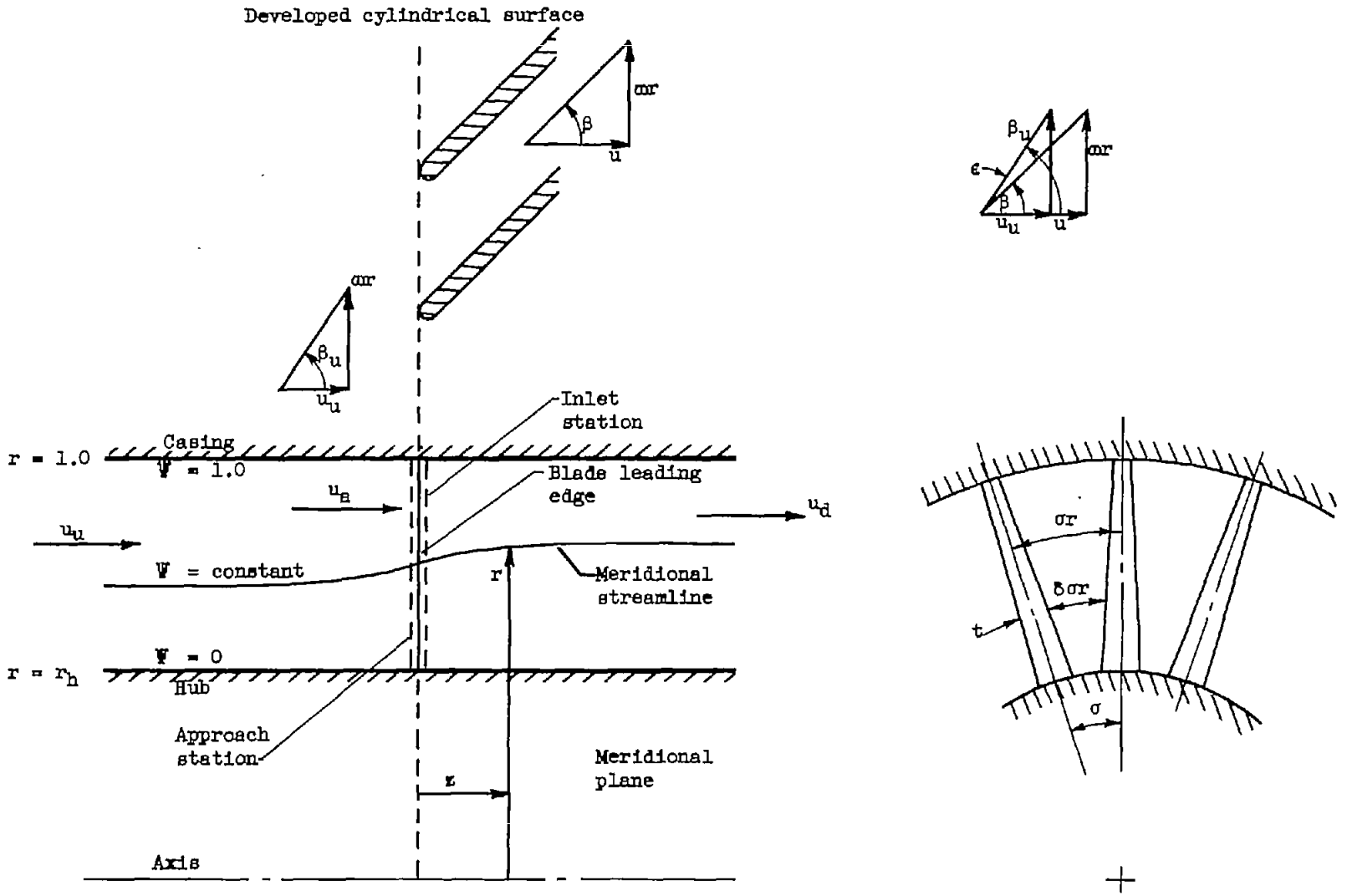

Figure 1. - Annulus of concentric circular cylinders with cascade of tapered blades.

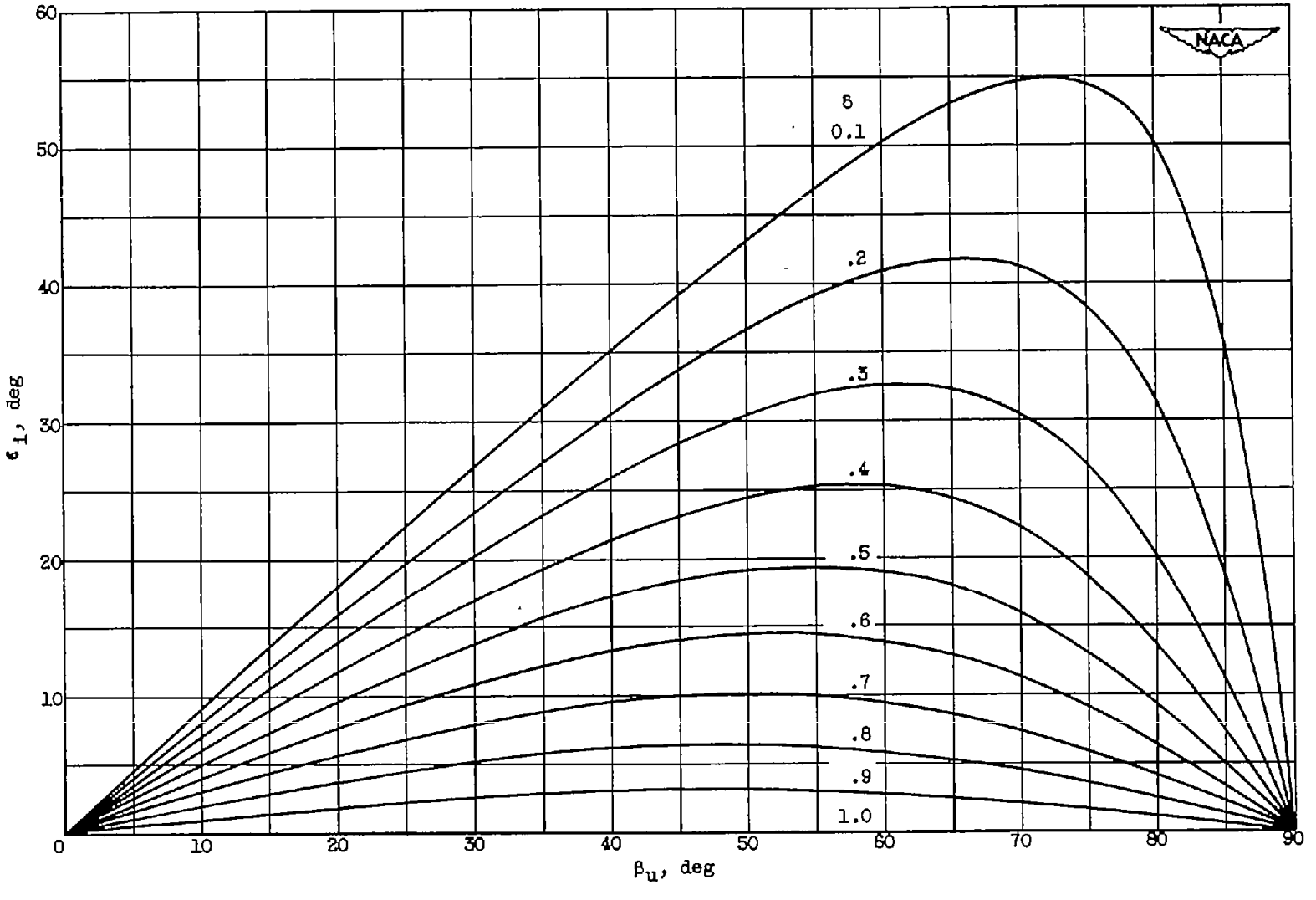

Figure 2. - Variation in inlet deviation angle ϵ_i with relative upstream angle β_u for various passage width ratios δ. Plane, incompressible flow; equation (15).

2975

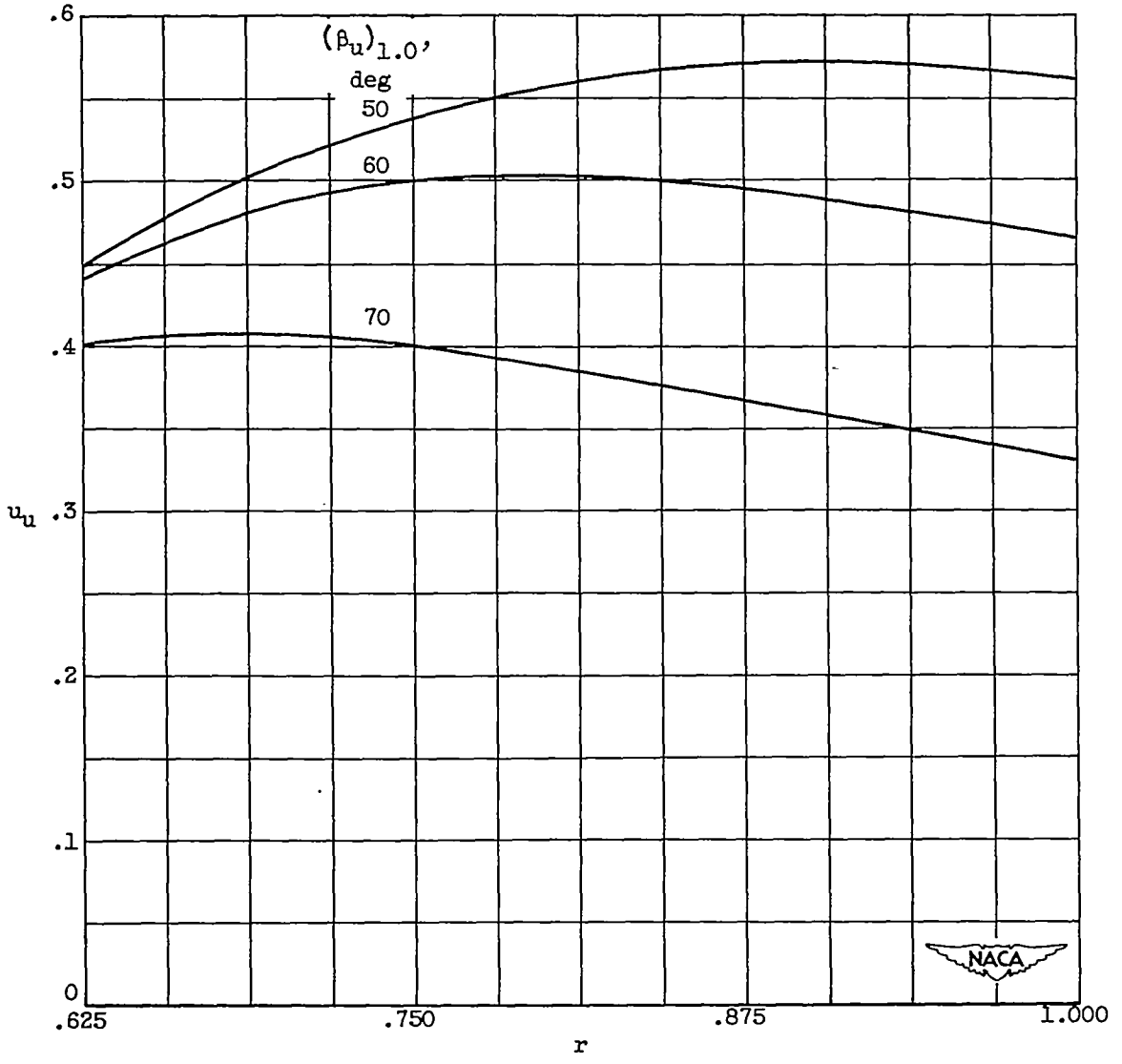

Figure 3. - Variation in u_u required at radius r for sonic velocity in inlet. Example V, equation (17).

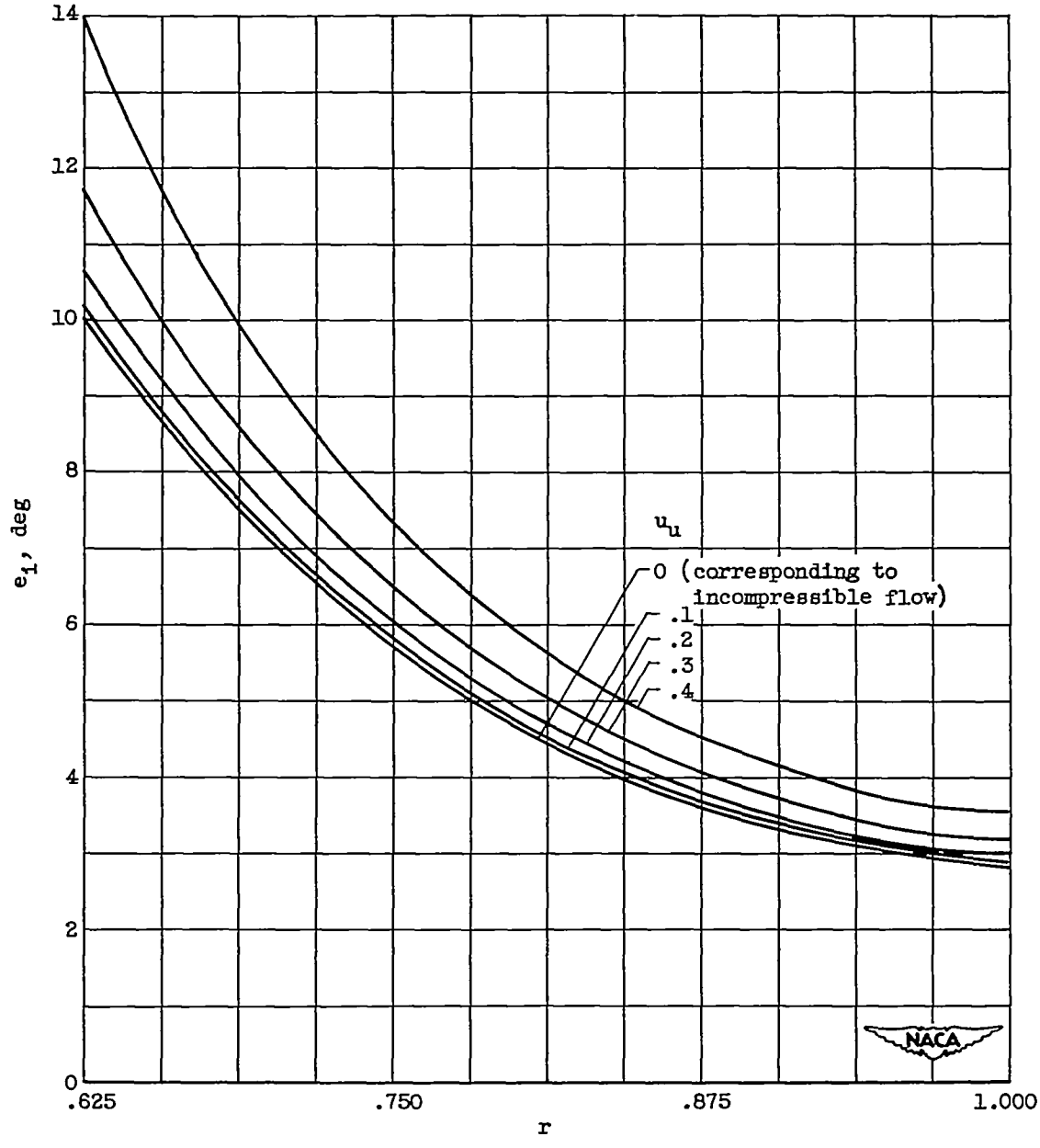

(a) $(\beta_u)_{1.0}$, 60°.

Figure 4. - Variation in inlet deviation angle e_i with radius r for example V with various values of $(\beta_u)_{1.0}$ and u_u. Equation (14).

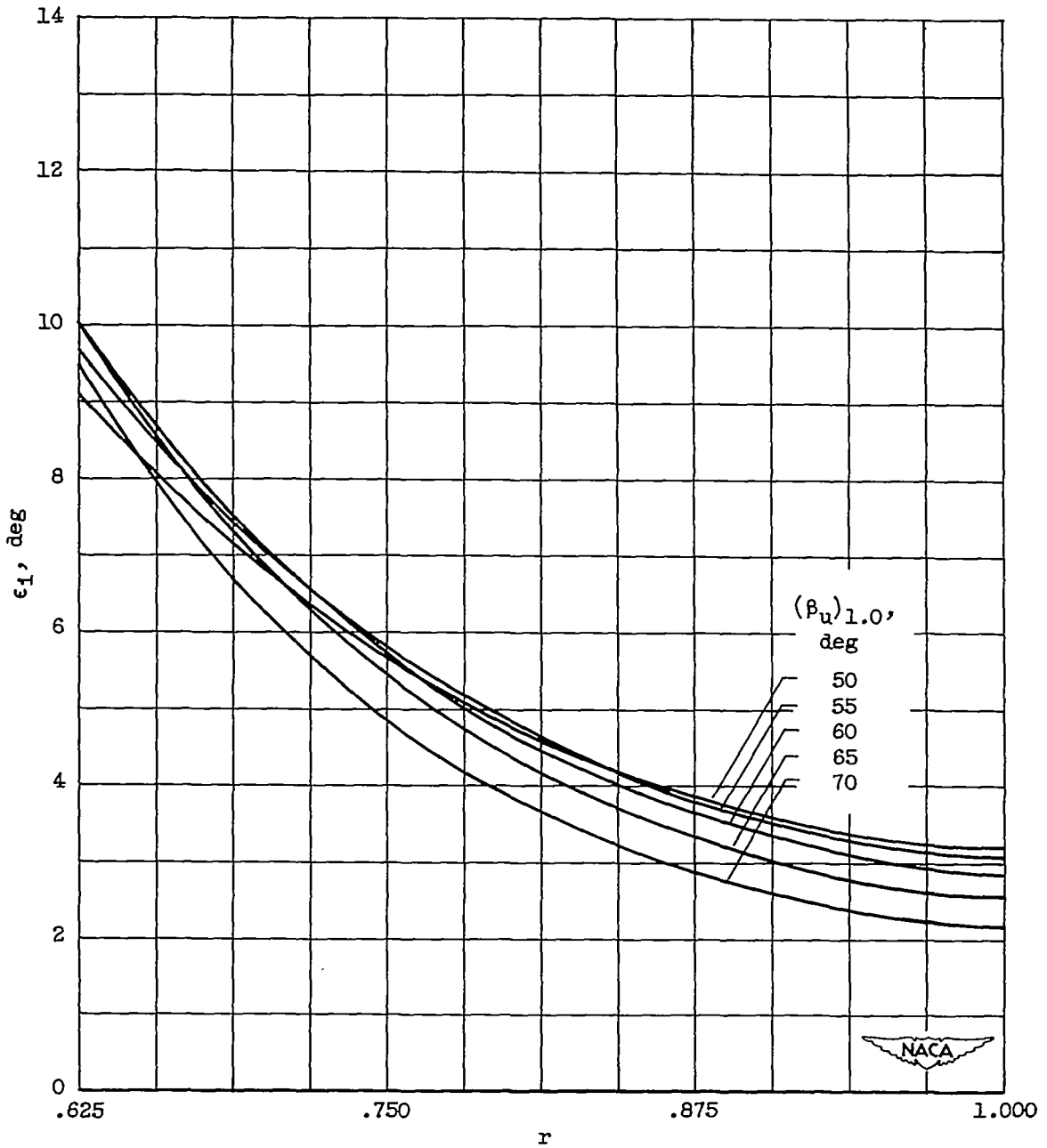

(b) u_u, 0 (corresponding to incompressible flow).

Figure 4. - Concluded. Variation in inlet deviation angle ϵ_1 with radius r for example V with various values of $(\beta_u)_{1.0}$ and u_u. Equation (14).

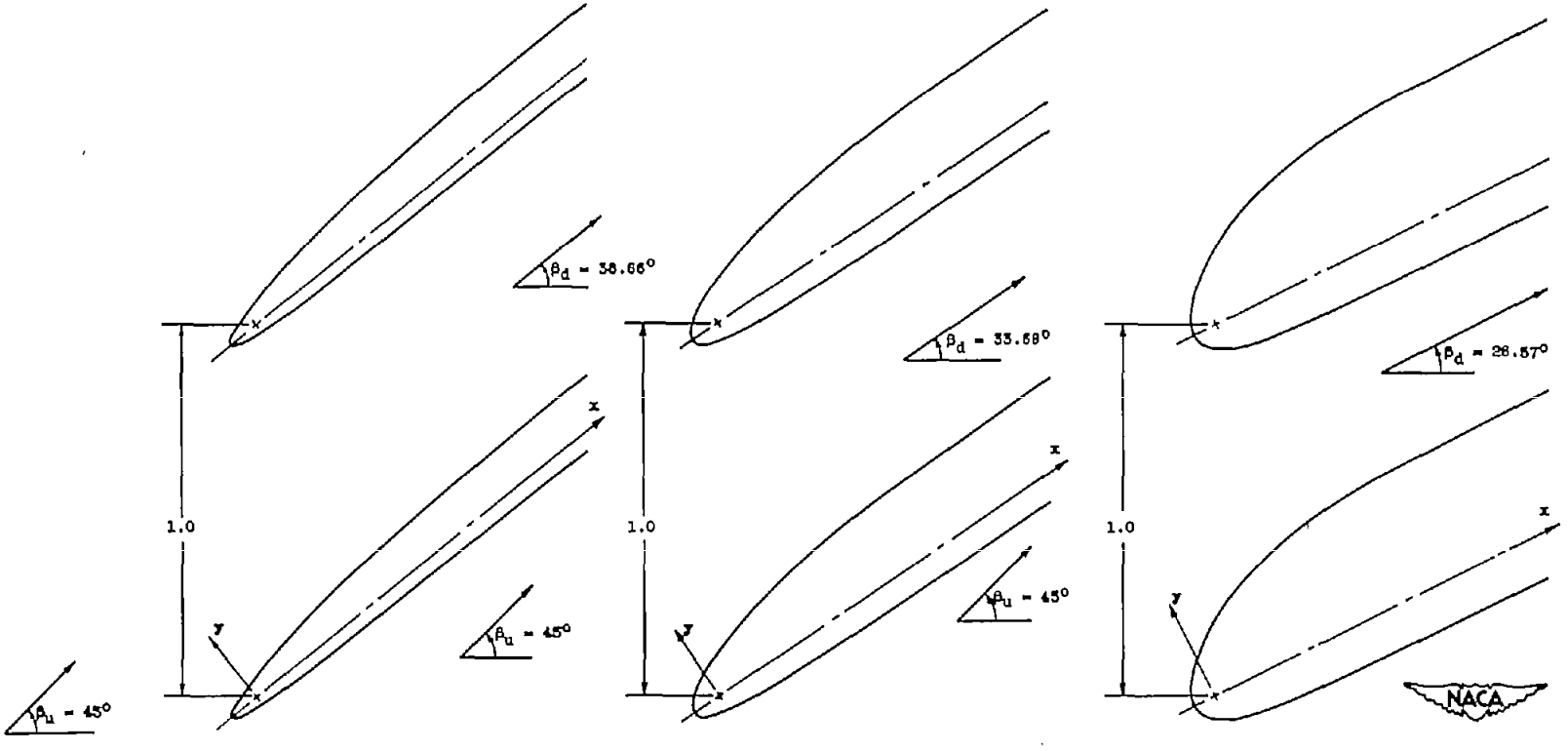

(a) Passage width ratio s, 0.8. (b) Passage width ratio s, 0.8887. (c) Passage width ratio s, 0.8.

Figure 5. - Shape of faired-nose leading edge for plane, two-dimensional, incompressible flow with zero blade loading.

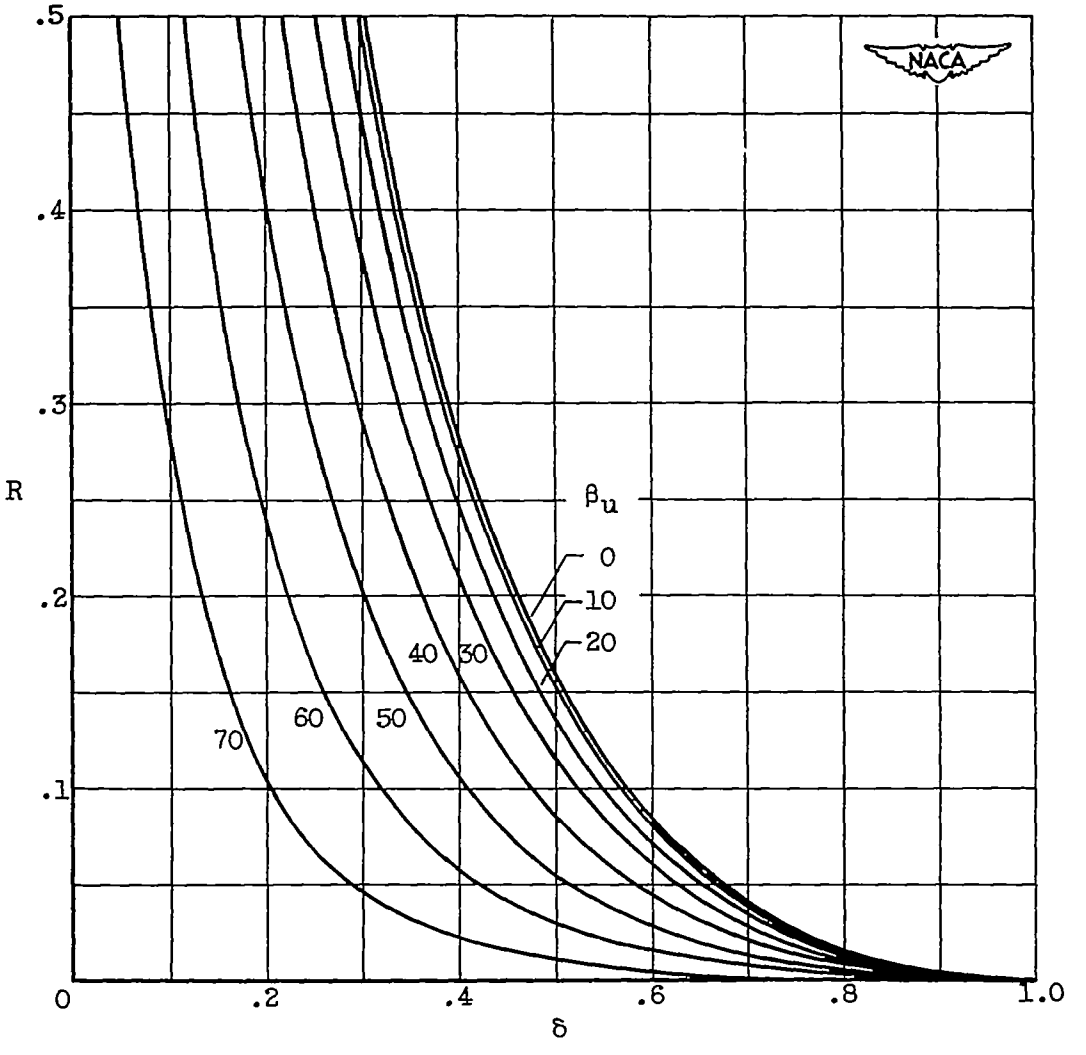

Figure 6. - Variation in nose radius R with passage ratio δ for various relative upstream flow angles β_u. Plane, two-dimensional, incompressible flow; equation (22).

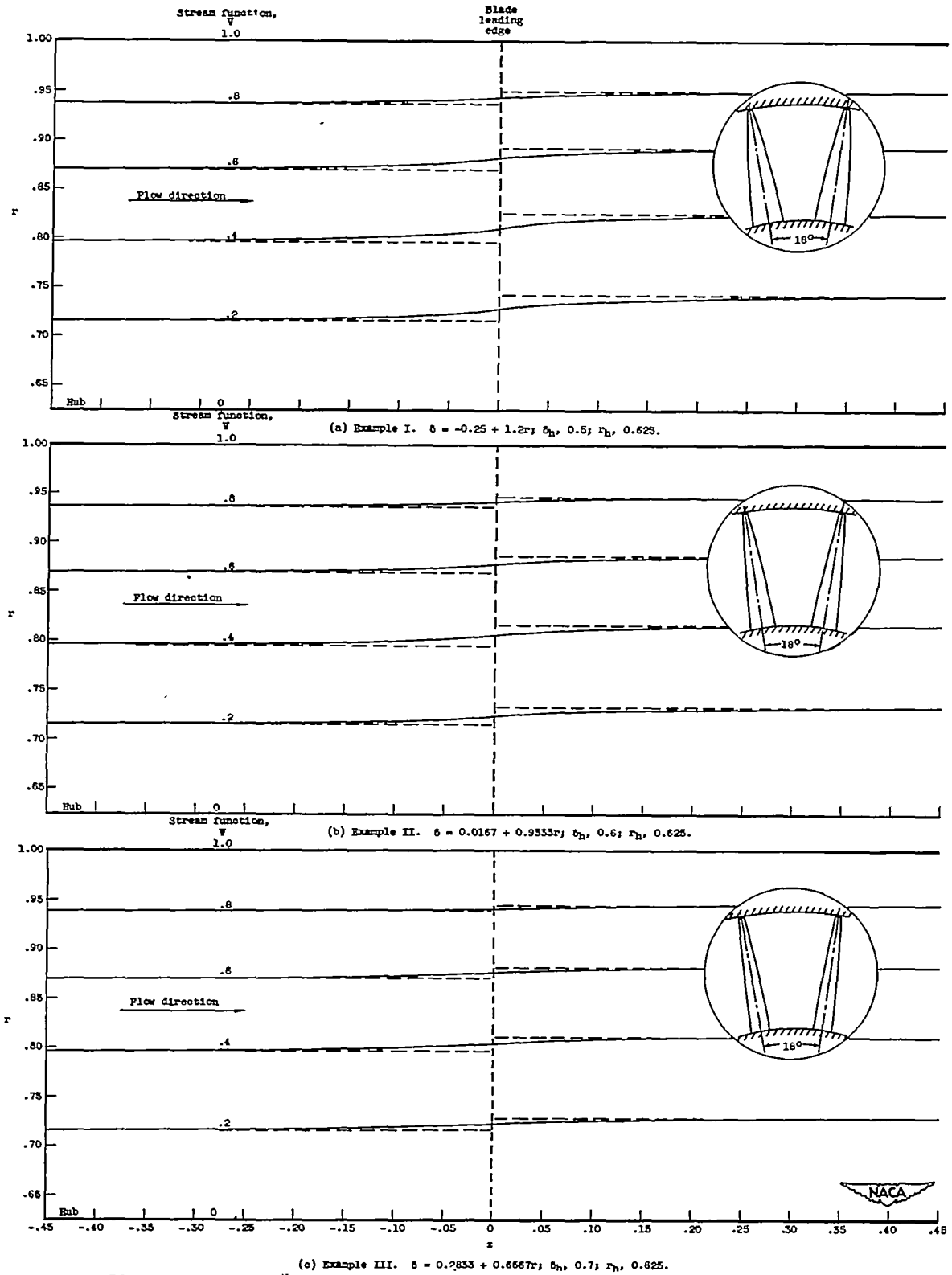

Figure 7. - Relaxation solutions for streamline distribution upstream and downstream of leading edge of entrance rotor-blade row with blade taper. Dashed lines show radial spacing of streamlines far upstream and far downstream of leading edge. $\delta_{1.0}$, 0.95; incompressible flow.

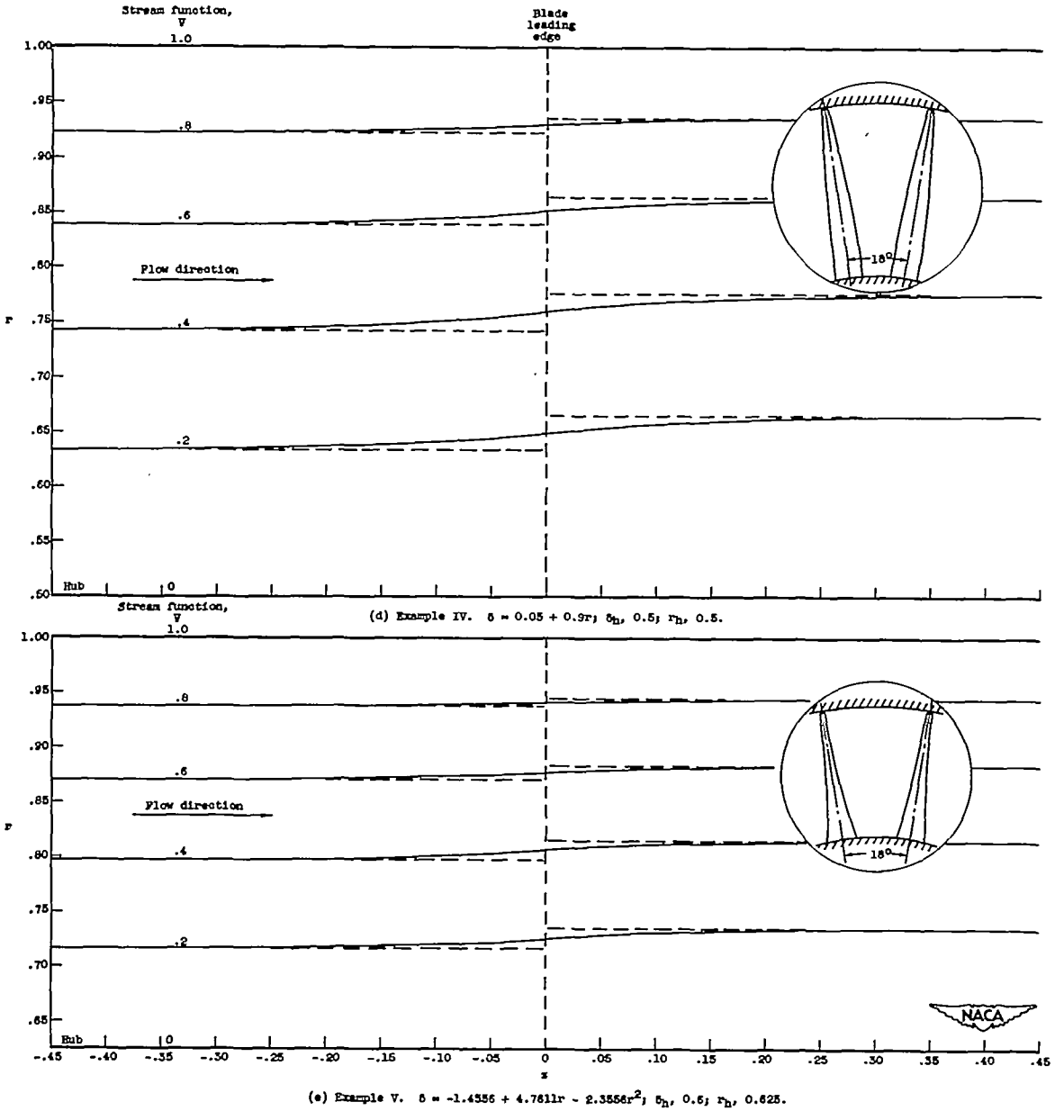

Figure 7. - Concluded. Relaxation solutions for streamline distribution upstream and downstream of leading edge of entrance rotor-blade row with blade taper. Dashed lines show radial spacing of streamlines far upstream and far downstream of leading edge. $\delta_{1.0}$, 0.95; incompressible flow.

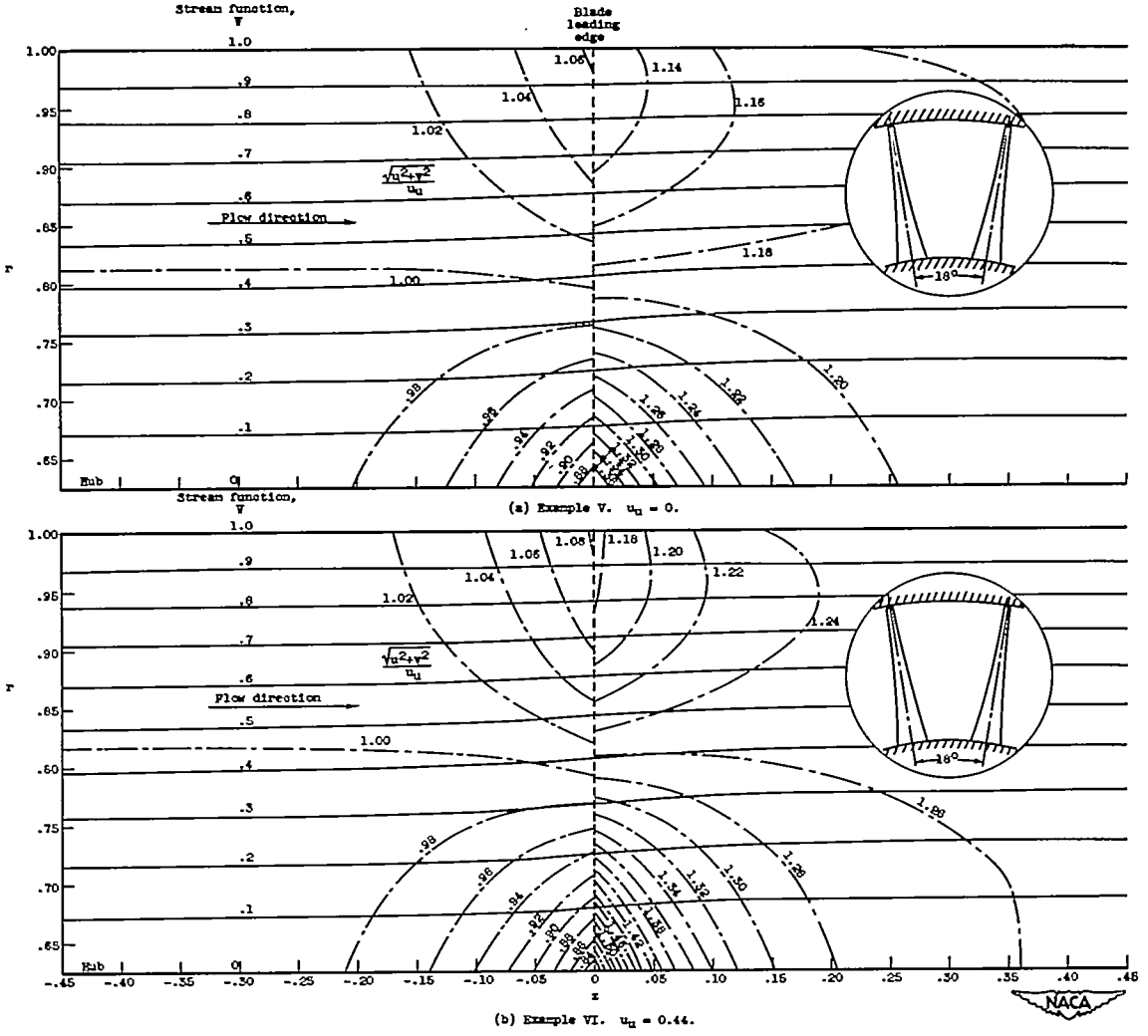

Figure 8. - Relaxation solutions for effect of upstream velocity u_u on streamlines and velocity ratio $\sqrt{u^2+v^2}/u_u$ distribution. $\delta_{1.0}$, 0.95; δ_h, 0.60; r_h, 0.625; $\delta = -1.4556 + 4.7611r - 2.3556r^2$; compressible flow.

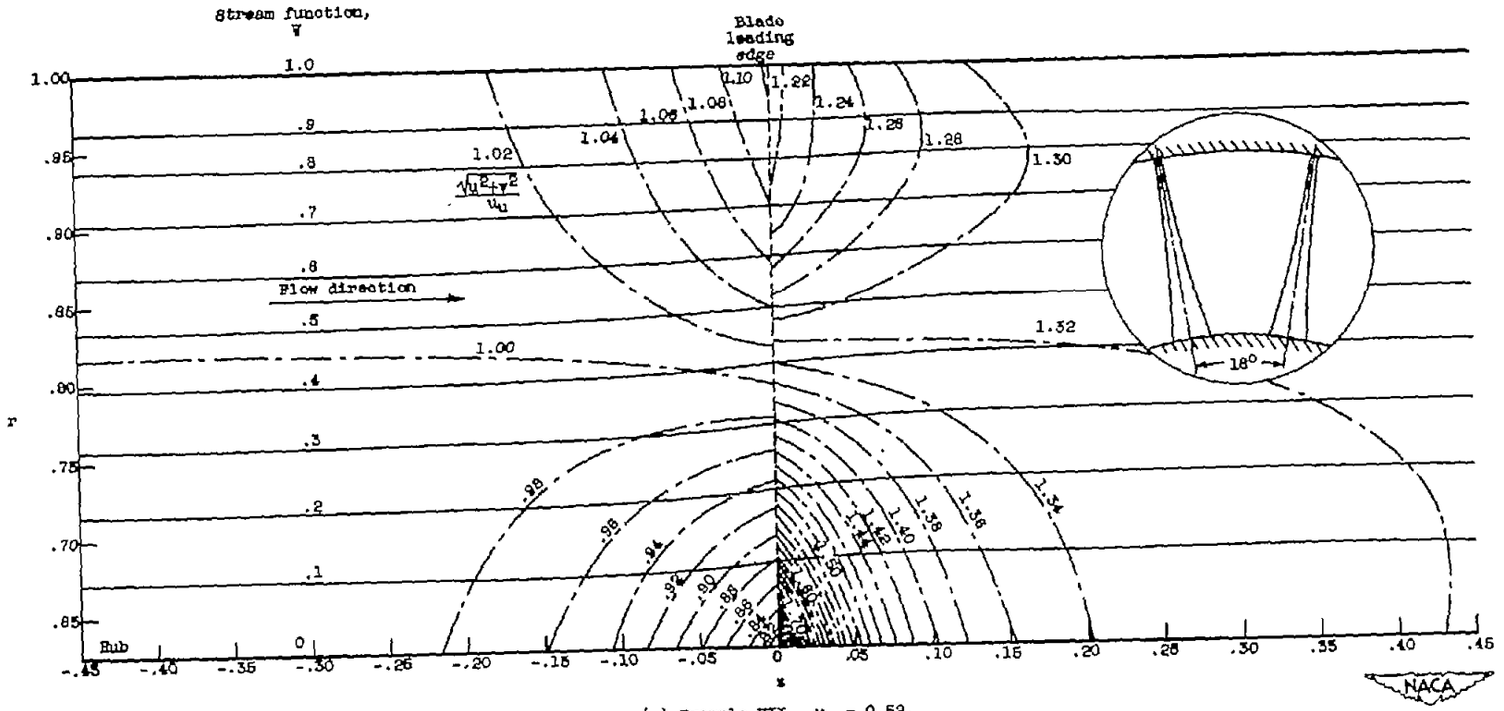

(o) Example VII. $u_1 = 0.52$.

Figure 8. - Concluded. Relaxation solutions for effect of upstream velocity u_1 on streamlines and velocity ratio $\sqrt{u^2+v^2}/u_1$ distribution. $\delta_{1.0}$, 0.95; δ_h, 0.80; r_h, 0.625; $\delta = -1.4558 + 4.7811r - 2.3558r^2$; compressible flow.

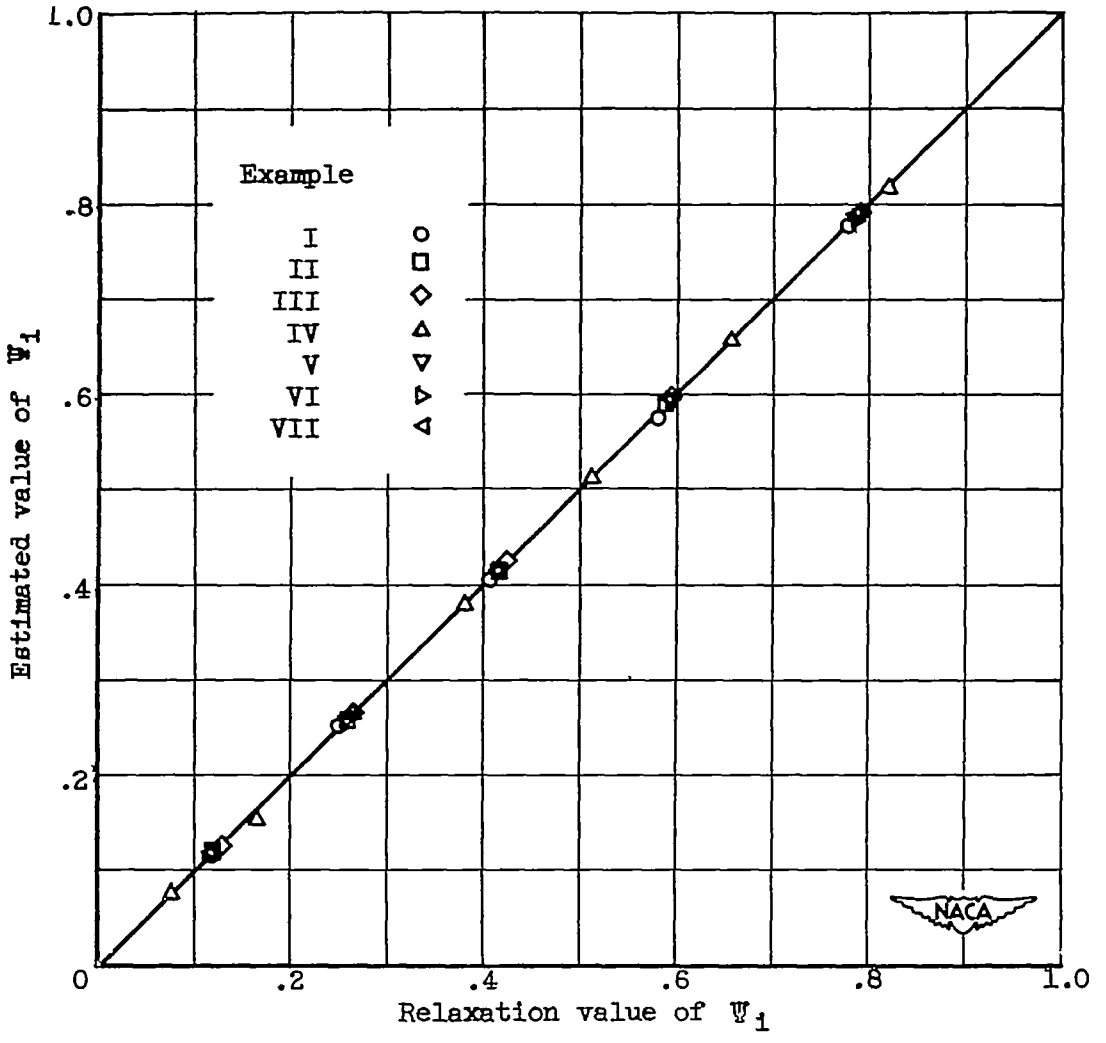

Figure 9. - Comparison of stream function Ψ_i obtained along leading edge of blade by relaxation solution with approximate stream function Ψ_i given by equation (10). Values of r_i: 0.625, 0.6875, 0.750, 0.8125, 0.875, 0.9375, and 1.000; in addition, 0.500 and 0.5625 for example IV.

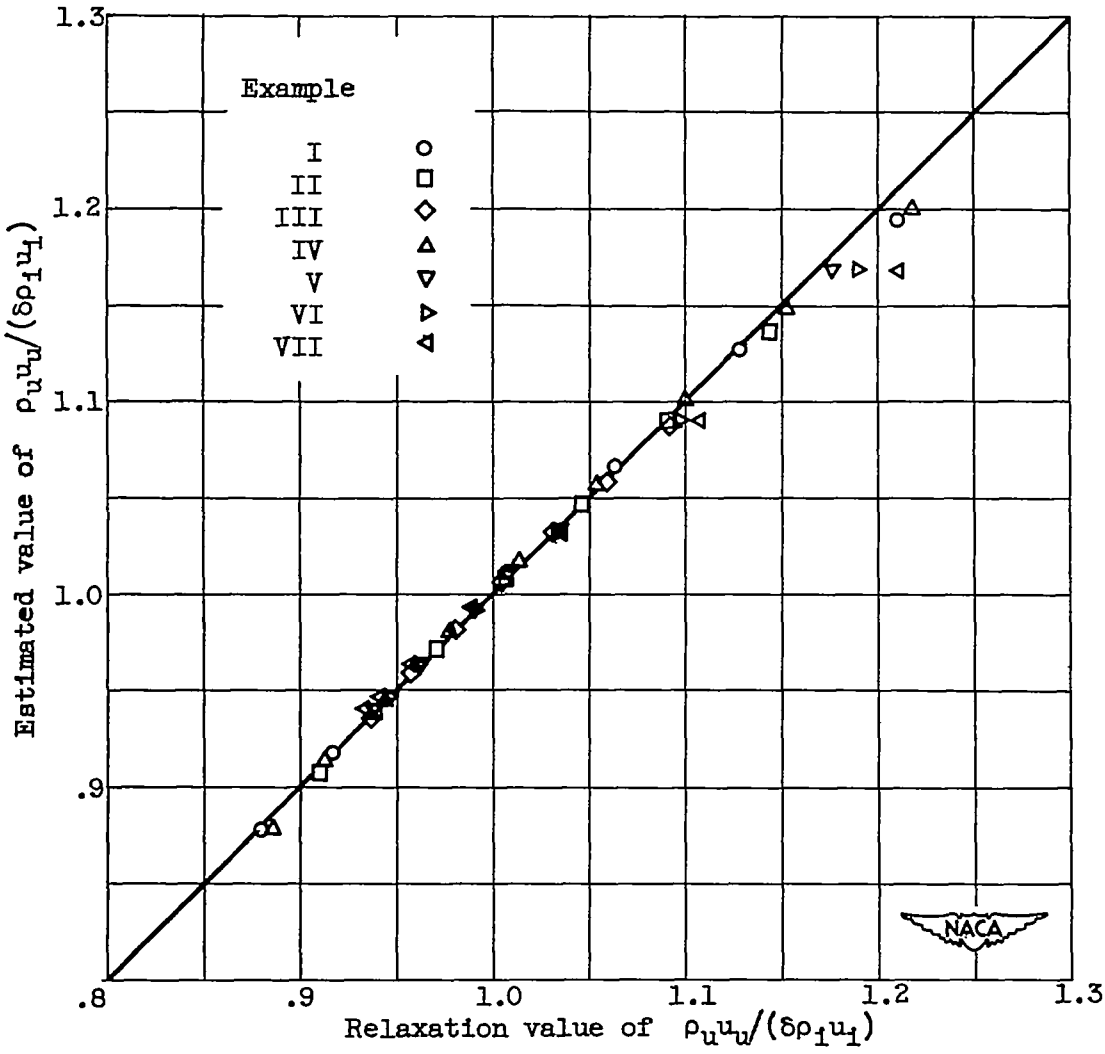

Figure 10. - Comparison of $\rho_u u_u/(\delta\rho_i u_i)$ obtained along leading edge of blade by relaxation solution with $\rho_u u_u/(\delta\rho_i u_i)$ given by equation (11). Values of r_i: 0.625, 0.6875, 0.750, 0.8125, 0.875, 0.9375, and 1.000; in addition, 0.500 and 0.5625 for example IV.

NACA-Langley - 8-19-53 - 1000